Particle Physics at CERN

Annual Report 2009

(SNF grants 200020-124377 and 206620-124379)

E. Aguiló, E. Alagöz, C. Amsler, A. Benelli, V. Boccone, W. Creus, S. de Visscher, M. Ivova,
B. Millán Mejías, P. Otyugova, C. Regenfus, P. Robmann, J. Rochet, T. Rommerskirchen,
A. Schmidt, L. Scotto Lavina, S. Steiner, D. Tsirigkas, and L. Wilke

V. Chiochia, C. Favaro, A. Jaeger, and H. Snoek

July 14, 2010

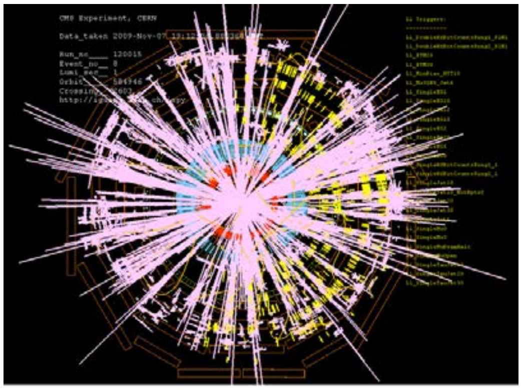

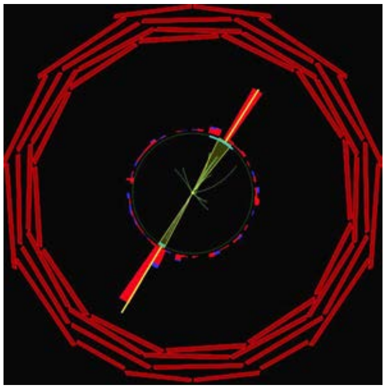

Physik-Institut der Universität Zürich
Winterthurerstrasse 190, CH-8057 Zürich, Switzerland

Contents

This report covers the activities of the Zurich group at CERN on CMS, the DIRAC and the ArDM experiments between 1 April 2009 and 31 March 2010. It does not include the activity of one of us (C. A.) contributing to the "Review of Particle Physics" (Particle Data Group). Further details on the group activities and publication reprints can be obtained from our home page, see http://cern.ch/unizh/.

The top left picture on the cover page shows one of the first collisions registered by CMS at 900 GeV in November 2009 and a Z^0-decay into e^+e^- at 7 TeV in March 2010 (right). The bottom picture shows our new dd-fusion source in our lab at CERN which delivers monoenergetic (2.45 MeV) neutrons for R&D in dark matter searches.

1 Particle physics with CMS

E. Aguiló, E. Alagöz[1], C. Amsler, S. de Visscher, M. Ivova, B. Millán Mejías,
P. Otyugova, C. Regenfus, P. Robmann, J. Rochet, T. Rommerskirchen, A. Schmidt,
S. Steiner, D. Tsirigkas[2], and L. Wilke[3]

V. Chiochia, C. Favaro, A. Jaeger, and H. Snoek

In collaboration with:
Paul Scherrer Institut (PSI) and the CMS Collaboration

1.1 Introduction

The silicon pixel detector is the innermost component of the CMS experiment [1] at the LHC. It allows a precise reconstruction of the directions of charged particles and the identification of displaced vertices from long-lived particle decays. The 53 cm long barrel pixel section, counting about 48 million channels, consists of three cylindrical layers at radii between 4.4 cm and 10.2 cm. Two endcap disks at each side of the barrel provide coverage up to large rapidities.

We were involved since 1995 in the design, construction and commissioning of the barrel pixel detector [1]. We have led prototype tests with CERN beams, measuring sensor performances before and after irradiation, such as position resolution, detection efficiency, charge sharing and Lorentz deflection. In addition, we have contributed to the development and commissioning of the readout chip. We have designed and built in the Institute workshop the mechanical and cooling structure and the two service tubes which provide coolant and power, and transfer the signals to and from the pixel detector. Details can be found in earlier reports and in various publications such as refs. [2, 3, 4].

After a commissioning phase with cosmic rays CMS started recording proton collisions in December 2009 at the center-of-mass energy of 900 GeV (fig. 1.1). During the run a world record center-of-mass energy of 2.36 TeV was achieved with the LHC. A first physics publication on multiplicity distributions has already appeared [5]. A run at 7 TeV has started in March 2010 (fig. 1.1) which is expected to last until autumn 2011, with the goal to reach an integrated luminosity of 1 fb^{-1}.

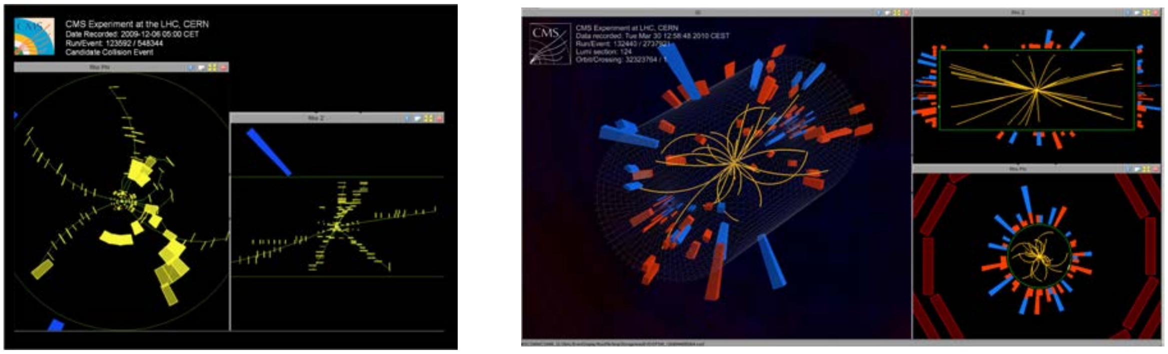

Figure 1.1: *Events displays of the first pp-collisions registered by CMS at 900 GeV in December 2009 (left) and at 7 TeV in March 2010 (right).*

---

[1] until 31 August 2009.

[2] until 31 August 2009.

[3] until 31 December 2009.

1.2 Commissioning of CMS silicon pixel detector with first collision data

As the CMS pixel detector plays a key role for several physics analyses, our first priority was to measure its performance with LHC collisions and to compare with expectations. Last year we performed several important measurements and calibrations, ranging from a measurement of the detector occupancy and position resolution to that of the Lorentz angle in the 3.8 T magnetic field.

First, background events such as beam-halo or beam-gas interactions have to be carefully removed during the offline selection. We have developed several rejection algorithms that are now employed in CMS analyses and have studied the dependence of the background rate on LHC operating conditions. In the near future we will also test the effects of beam tuning on the background rate.

One of the most important benchmarks is the occupancy which provides estimates of the detector noise. The comparison with expectations from event generators is also very important to fine-tune phenomenological parameters such as parton showers and multiple partons interaction, which influence charged particle production at very low momenta, and can produce a large number of hits in the innermost layers of the pixel detector. The pixel detector occupancy was measured at 0.9 TeV and 2.36 TeV center-of-mass energies for the barrel section (see fig. 1.2), and for single barrel modules (or blades in the endcap sections). The average occupancy is in very good agreement with expectations, with discrepancies generally smaller than 5%. However, fine tuning of the Monte Carlo generators will be needed as no fitting to data was attempted so far for LHC energies.

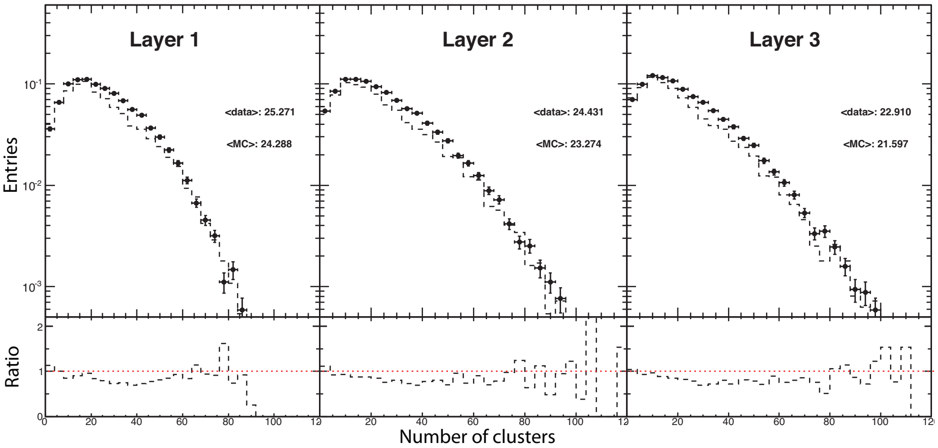

Figure 1.2: *Measured (dots) and simulated pixel hit multiplicities in the three barrel layers at 900 GeV. The bottom plots show the ratios between measurements and simulations.*

Charge collection was also compared to Monte Carlo simulation (fig. 1.3). The pixel cluster charges were normalized to the path lengths in the silicon sensors. We observed excellent agreement with simulation for the peak position, width and tails of the distribution, hence have a very good understanding of the analogue readout chain and charge calibration.

A measurement of the position resolution was performed using first collision data. We used pairs of consecutive hits along trajectories in the overlap regions between adjacent modules of a given layer, and calculated the differences in hit positions Δx_{hit} (Δy_{hit}) along the transverse (longitudinal) direction. We then computed the double difference, Δx (Δy) between Δx_{hit} (Δy_{hit}) and the differences Δx_{pred} (Δy_{pred}) between the expected positions from trajectory extrapolation. The double difference distribution was then fitted with a Gaussian and the uncertainty on the predicted position quadratically subtracted from the width, to recover the intrinsic hit resolution. The results are shown

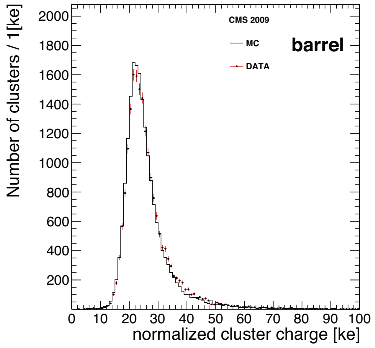

Figure 1.3: *Measured (dots) and simulated cluster charge distribution in the barrel pixel detector.*

in fig. 1.4. Each point represents the resolution measurement for a different pair of overlapping modules. The mean value is shown as a solid line in the plot. The r.m.s. resolutions are 12.9±3.0 μm along the transverse coordinate (x) and 32.4±4.9 μm along the longitudinal coordinate (y). The same technique on a Monte Carlo sample gives results in agreement with data.

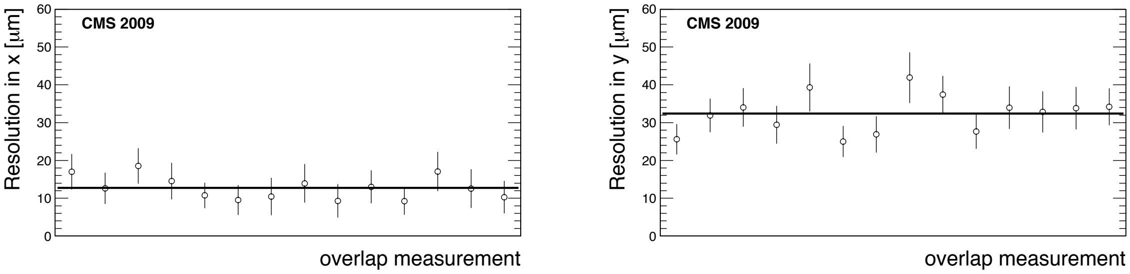

Figure 1.4: *Position resolution for the barrel detector along the transverse (left) and longitudinal (right) coordinates. Each point corresponds to a pair of overlapping modules, calculated from more than 20 crossing tracks. The solid line shows the average resolution.*

Ionization charges produced by particles traversing the pixel sensors drift under the combined electric and magnetic fields. The ensuing Lorentz angle between drift direction and electric field leads to a systematic shift of the hit position that has to be corrected. The shift depends on various experimental conditions such as bias voltage, temperature and irradiation, and has therefore to be measured in-situ and monitored. Measurements of the Lorentz angle with the barrel pixel detector were performed with the 2009 cosmic ray run (CRAFT09 [6]). Since detector operating conditions (bias voltage, temperature, etc.) were different from the 2008 data (CRAFT08), a different Lorentz angle was expected [7, 8]. The angle was measured by finding the minimum of the mean cluster size distribution, measured as a function of the track incidence angle [9]. The result (first row in Table 1.1) is in good agreement with the prediction from the PIXELAV simulation [10]. As expected, the measured value (fig. 1.5, left) was about 2° lower than for CRAFT08.

Sample	**Method**	**Measured** $\tan\theta_L$	**PIXELAV simulation**
cosmic rays	cluster size	0.4071±0.0020(stat)	0.3972±0.0030(stat)
collisions	grazing angle	0.3985±0.0005(stat)	0.4006±0.0005(stat)
collisions	cluster size	0.4094±0.0016(stat)	0.4113±0.0048(stat)

Table 1.1: *Lorentz angle θ_L in the barrel pixel detector determined with two different techniques, using cosmic ray tracks and minimum bias events from LHC collisions.*

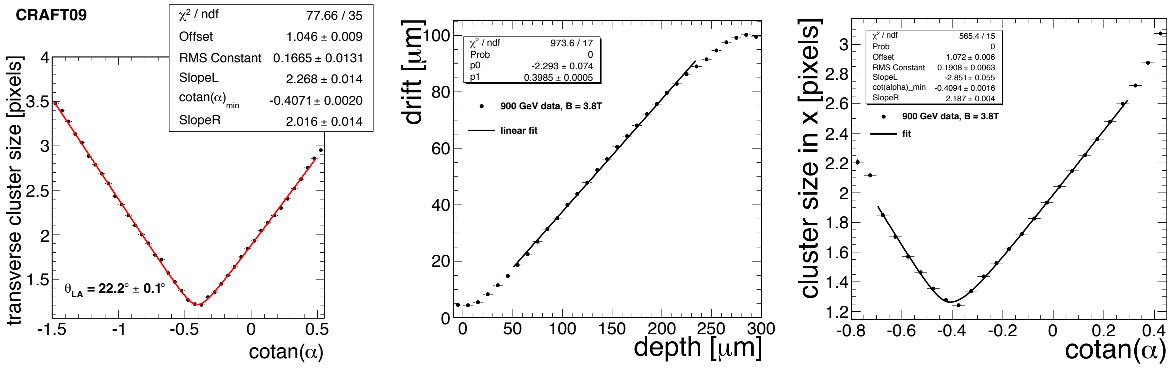

Figure 1.5: *Measurements of the Lorentz angle in the 3.8 T magnetic field. Left: pixel cluster size as a function of incidence angle from cosmic rays. Middle: transverse cluster displacement as a function of sensor depth for minimum bias events. Right: cluster size as a function of incidence angle for minimum bias events. Solid lines represent fits to the data points.*

The measurements were repeated with tracks from proton collisions using the "grazing angle" technique [11]. The transverse cluster displacement was measured as a function of production depth from tracks with shallow impact angles (fig. 1.5, middle). The large number of low momentum tracks at 900 GeV also allowed a measurement using the cluster size technique (fig. 1.5, right). In all cases excellent agreement was obtained between experimental results and PIXELAV simulation (Table 1.1).

1.3 Spatial alignment of the silicon pixel and strip tracker

The alignment of the CMS tracker is a complex task in view of the very large number of silicon sensors (about 15'000) and their excellent position resolution. Two alignment algorithms are being used: the *Hit and Impact Point (HIP)* algorithms used by the Zurich groups, and the *Millepede* approach. While the latter is suitable to detect large movements, the former can lead to very precise positions for small distances. Hence the best alignment precision is obtained by applying the *HIP* algorithm starting on sensors positions previously obtained with the *Millepede* algorithm. We collected a large sample of cosmic ray tracks in summer 2009 before LHC operation. The data allowed a precise spatial alignment of the tracker after the hardware interventions of the previous year. The analysis of alignment data taken with pp-collisions is in progress. The alignment of the pixels can be achieved with a typical precision of 2 μm (4μm) in the transverse (longitudinal) directions.

1.4 Improvements to the pixel hit reconstruction

Searches for the Higgs boson or new particles beyond the Standard Model (such as SUSY), depend heavily on the identification of τ-leptons and b-quark jets. For example, the τ-lepton decays into three charged pions (and an invisible neutrino) with a branching ratio of about 10%. Since the transverse momentum of the τ-jet is large compared to the τ mass, the decay pions emerge in a strongly collimated jet in which the charged tracks stay in close proximity. The larger the τ momentum, the more strongly collimated the three tracks, which makes them inseparable when the pixel hits merge into one large cluster. This occurs in the innermost pixel layer when the opening angle between the two trajectories is below 5 mr, which corresponds to a transverse momentum of 150 GeV/c for a typical 3-prong decay. This effect deteriorates the measurement of the particle trajectories and the reconstruction of the τ mass. Thus, an excellent spatial resolution is needed for τ reconstruction.

The measured cluster charge and track impact angles can be used to discriminate merged hits from isolated hits. Figure 1.6 shows a simulation of the pixel cluster charge distribution, corrected for the traversed path length, for merged and isolated clusters produced by τ decays. Merged clusters produce satellite peaks at twice or three times the minimum ionizing energy deposit and can therefore be recognized.

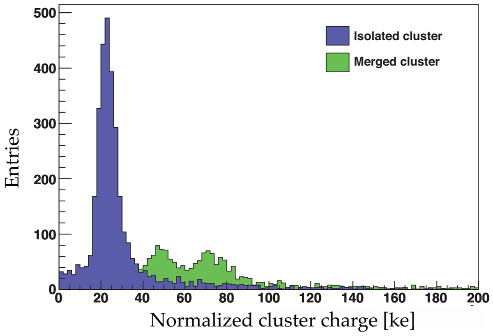

Figure 1.6: *Pixel cluster charge distribution (corrected for impact angle) for hadronic τ decays. The blue histogram shows isolated clusters, while the green histogram shows the merged hits.*

From simulations we have also shown that the splitting of merged clusters has an impact on the track parameter resolutions and on the b-jet selection efficiency. We are therefore implementing a cluster splitting technique in the pixel hit reconstruction software which we intend to use for Higgs searches in τ decays.

1.5 Improvements to b-quark tagging techniques

The b-tagging algorithms in the CMS fast Monte Carlo simulation [12] are under our responsibility. The fast b-tagging uses the same algorithms as the full detector simulation and reconstruction. The disadvantage is that the agreement between fast and full (GEANT4 based) detector simulations is not perfect in all regions of phase space. Various improvements have therefore been implemented:

- pixel hit merging: since the track reconstruction in the fast simulation does not include the step of pattern recognition, faked tracks are not reproduced. Thus, detector effects such as hit sharing between tracks or cluster merging (section 1.4), are not simulated. To estimate the contribution from these effects, a pixel hit merging algorithm was implemented in the fast simulation and tracks with shared hits were removed in the full detector reconstruction.

- material effects: particles traversing the tracking detectors are subject to multiple scattering, nuclear interactions and conversions (for photons). The fast simulation uses a simplified detector geometry and the material budget is tuned according to the amount of photon conversions obtained from the full simulation. This simplified geometry potentially introduces biases which affect the tracking performance in the inner layers. These effects have been investigated by varying the thickness of materials.

- pixel hit parameterization: the resolution of pixel hits was parameterized and tuned according to the full detector simulation.

Figure 1.7 displays the performance of the secondary-vertex based b-tagging algorithm, without (left) and with the new features (middle). Depending on b-tagging efficiency, the misidentification rate increases by up to a factor of two, and agrees almost perfectly with the full simulation.

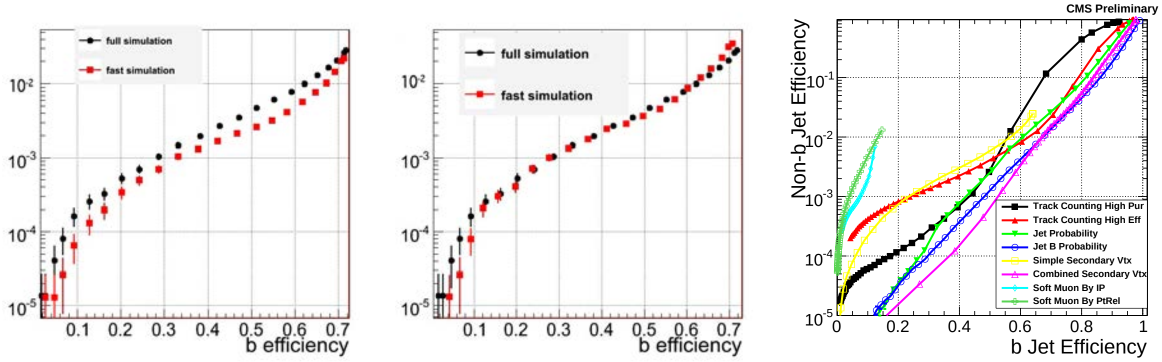

Figure 1.7: *Misidentification rate of the "secondary vertex" b-tagging algorithm vs. b-tagging efficiency, before (left) and after (middle) the improvements described in the text. Right: Mistagging efficiency of all CMS b-tagging techniques vs. b-tagging efficiency (from refs. [13, 14]).*

A comparison of the CMS b-tagging algorithms is shown in fig. 1.7 (right). During the 2010 runs we will monitor of the physics observables used in the b-tagging algorithms and determine the algorithm performances with data-driven methods.

1.6 Studies of $B_s \to (J/\psi)\phi$ and B_c-decays

The lifetime of the B-mesons is relatively long and the CMS pixel detector can determine B-decay vertices precisely. This reduces the background substantially and facilitates measurements of the B_s mass and mean life, and the measurement of B_s mixing parameters, such as the width difference between the B_s^H and B_s^L mass eigenstates, together with the CP violating weak phase, which is sensitive to physics beyond the Standard Model.

Physics involving the b-quark will be among the first studies to be performed with LHC data. We have studied in detail the decay channel $B_s \to (J/\psi)\phi \to (\mu^+\mu^-)K^+K^-$ [9, 15]. B_s-decays into J/ψ are selected during data taking using a di-muon trigger. Events are further selected offline by requiring two opposite sign muons from the J/ψ and a common vertex from the J/ψ and ϕ particles, and cutting on the transverse momentum of the kaons from ϕ decay. To reconstruct $B_s \to (J/\psi)\phi$ additional quality cuts are applied on the observables and a kinematic fit is applied. Figure 1.8 shows the factor of two improvement to the reconstructed B_s mass width obtained with the kinematic fit.

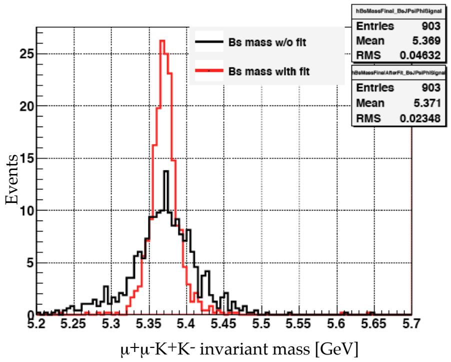

Figure 1.8: *Mass distribution in the B_s region with and without kinematic fit (simulation).*

We will observe the $B_s \to (J/\psi)\phi$ decay already with an integrated luminosity of 1 pb^{-1}. We will then determine the B_s mass and mean life with 10 pb^{-1}, measure the CP-even and CP-odd components with more than 50 pb^{-1}, and extract the CP weak phase difference with more than 100 pb^{-1}. Figure 1.9 shows the reconstructed B_s invariant mass for 1 pb^{-1} and 10 pb^{-1}, respectively (from two analyses with slightly different cuts). The well measured channel $B_d \rightarrow (J/\psi)K^*$ was selected as calibration channel. Figure 1.9 (right) shows the reconstructed B_d-mass using the same analysis code as for the B_s case (middle plot).

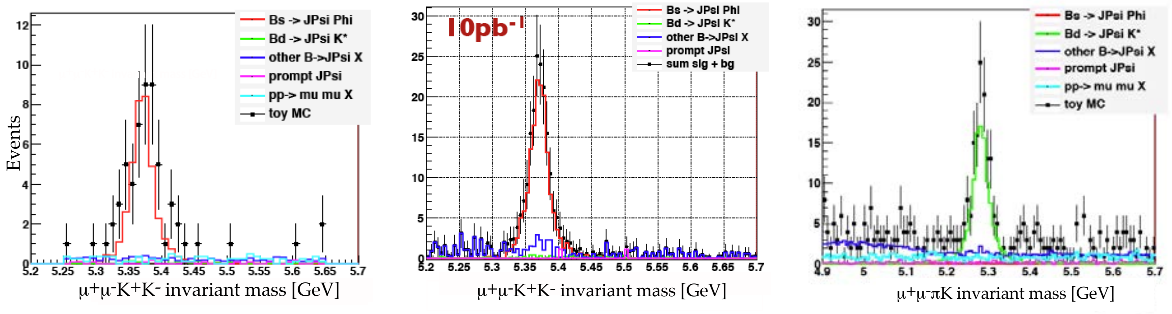

Figure 1.9: *Left: Reconstructed* B_s*-mass spectrum for 1pb*$^{-1}$ *at 10 TeV. Middle: Reconstructed* B_s*-mass spectrum for 10 pb*$^{-1}$*. Right: Reconstructed* B_d*-mass spectrum for 1pb*$^{-1}$.

The B_c-meson is unique in that it is made of two different heavy quarks (b and c). We have started analyses to measure its mass and lifetime in two promising decay channels: $B_c^{\pm} \rightarrow J/\psi\ \rho^0\ \pi^{\pm}$ and $B_c^{\pm} \rightarrow J/\psi\ \rho^{\pm}$. The cleaner J/ψ-decay is into $\mu^+\mu^-$, but decays into e^+e^- pairs are also under investigation. In the first case, the ρ^0 decays into two charged pions, hence five tracks are associated to the same secondary vertex. In the latter case, the ρ^+ decays into a neutral and a charged pion, so three tracks and one electromagnetic cluster are produced.

1.7 Modeling of Higgs and jet production at the LHC

One of the main motivations for the LHC physics program is the study of the electroweak symmetry breaking mechanism and the Higgs boson discovery. The direct production of the Higgs boson via a top loop coupling to the incoming gluons has the largest cross-section, and hence is the most promising discovery channel, in particular via decays into two vector bosons. The survey of the different Higgs boson signatures above the Standard Model background will rely on data-driven studies, but also on comparison with Monte Carlo expectations.

For years, efforts have been made to develop Monte Carlo programs capable to model the collisions as accurately as possible, using both fixed order perturbative calculations and by merging matrix-element and parton-shower algorithms. Using the generators *Herwig, HNNLO*, *Madgraph / Madevent*, *MC@NLO, POWHEG* and *Sherpa* [16], one of us participated in the study of Higgs boson production via gluon-gluon fusion We have provided results using a jet merging technique (K_t-*MLM*) implemented in *Madgraph / MadEvent*. While a minimal set of parameters was chosen to be fixed for all simulations (parton densities, t-mass, center-of-mass energy), no detailed tuning was performed. The predictions from event generators are shown in fig. 1.10, for both rapidity and transverse momentum of the Higgs boson [16].

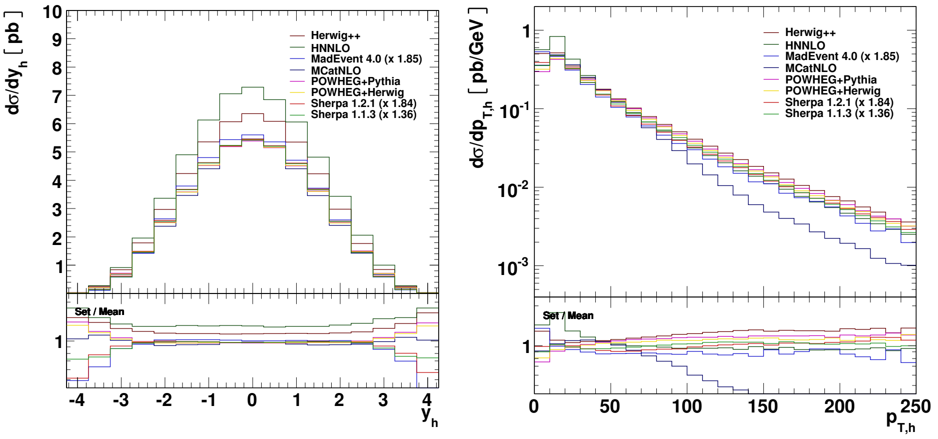

Figure 1.10: *Rapidity (left) and transverse momentum distributions (right) of the Higgs boson for LHC collisions predicted by different Monte Carlo simulations (from [16]).*

1.8 Search for Supersymmetry (SUSY) in multi-jet final states

In previous annual reports we reported on SUSY decays into 2 jets, no missing lepton and large missing energy. In 2009 the Monte Carlo study of Supersymmetry in di-jet events [17] was refined and extended to higher jet multiplicities [18]. Other approaches to reduce background have been studied and compared in terms of signal significance and robustness against systematic uncertainties. The basic selection for SUSY searches in hadronic final states relies on missing transverse energy. The corresponding cut is very effective in rejecting a large part of the QCD multi-jet background. Apart from the missing transverse energy M_T, another variable based on the global transverse thrust is useful, $Th\Delta\Phi$ [19]: The direction of the thrust axis is used to combine all jets in an event into two pseudo-jets emitted into two hemispheres. The variable $Th\Delta\Phi$ is then the angle between the two pseudo-jets in the transverse plane.

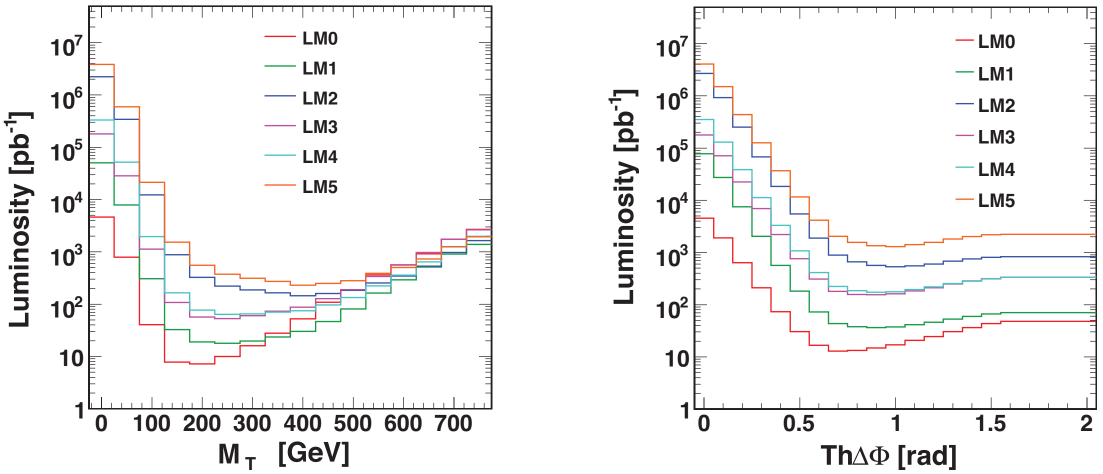

Figure 1.11: *Integrated luminosity required for SUSY discovery as a function of cuts on M_T (left) or $Th\Delta\Phi$ (right) for various points of the mSUGRA parameter space (from ref. [21]).*

Ignoring in a first step systematic uncertainties, the required minimum luminosity for a 5σ discovery of SUSY beyond Tevatron reach [20] is about 10 pb^{-1} (fig. 1.11). Systematic errors are due to uncertainties in the jet energy scale and the azimuthal angle. They were studied in detail and found to lead to an increase of the required minimum luminosity by about a factor two to three, depending on whether the $Th\Delta\Phi$ or the M_T cut is used.

1.9 Upgrades of the computing infrastructure

We have assembled a computing cluster (TIER4) for our group at CERN, which is regularly upgraded. The computing cluster proved to be essential to achieve prompt physics results, a clear asset in the early phases of data analysis, when the data load will not be too heavy. In 2009 five additional blades were installed for a total of 20 (3.3 GHz) CPU cores. The storage capacity was expanded to 50 TB by adding a new 14 TB disk array. The network was submitted to a major revision and the GB Ethernet switches were replaced with a 10 GB device. One additional 4 GB FiberChannel switch was installed. For the CMS data taking during 2010, new software releases based on Scientific Linux 5 (SLC5) will be used to benefit from improvements in C++ compilers. The current SLC4 will be deprecated. All of our machines are in the progress of being updated to SLC5.

1.10 Preparation for future upgrades of the CMS pixel detector

As a consequence of the latest LHC schedule review, the replacement of the current pixel system was postponed to the years 2016/17. Major upgrades are foreseen for the detector layout with the addition of a fourth barrel layer and a third disk in both endcap sections. The material thickness will be reduced by up to a factor of two in the central tracking region, thanks to new readout electronics and the evaporative cooling technique. The 0.13 μm CMOS technology for the front-end chip in the innermost layers is currently under evaluation. This technology allows a reduction of the pixel cell size, with corresponding improvements to the position and track resolutions in dense jets.

We performed a preliminary Monte Carlo study of the expected detector performances. The resolution on the hit position was studied as a function of pseudorapidity and cluster size with a sample of simulated muons. The resolution of the four track parameters that are measured by the pixel detector, namely the angles θ and ϕ, and the transverse and longitudinal impact parameters d_0 and d_z was also studied. As expected, the precision of track reconstruction is dominated by multiple scattering at low momenta, reaching an asymptotic value of $\sim$10 μm, respectively $\sim$30 μm, on the two impact parameters at high momenta. Estimates of the detector occupancy and b-tagging performance will be performed on a sample of simulated collisions events, and various pixel cell sizes will be compared.

References

[1] S. Chatrchyan *et al.* (CMS Collaboration), Journal of Instrumentation **3** (2008) S08004
[2] Y. Allkofer *et al.*, Nucl. Instr. Meth. in Phys. Res. **A584** (2008) 25
[3] V. Chiochia *et al.*, Nucl. Instr. Meth. in Phys. Res. **A568** (2006) 51
[4] A. Schmidt *et al.*, Journal of Instrumentation **4** (2009) P05003
[5] S. Chatrchyan *et al.*, (CMS Collaboration), Journal of High Energy Physics **02** (2010) 041
[6] S. Chatrchyan *et al.* (CMS Collaboration) Journal of Instrumentation **5** (2010) T03007
[7] A. Dorokhov *et al.*, Nucl. Instrum. Meth. in Phys. Research **A530** (2004) 71
[8] A. Dorokhov *et al.*, Nucl. Instrum. Meth. in Phys. Research **A560** (2006) 112
[9] L. Wilke, PhD Thesis, University of Zurich (2009)
[10] M. Swartz, Nucl. Instrum. Meth. **A511** (2003) 88
[11] L. Wilke, V. Chiochia, T. Speer, CMS Note 2008/012
[12] A. Schmidt, IEEE Nuclear Science Symposium Conference Record **N37-4** (2008) 2795

[13] W. Adam *et al.*, CMS Analysis Note 2009/085 and CMS PAS BTV-09-001.

[14] A. Schmidt, Proc. of Science (EPS-HEP 2009) 439

[15] K. Prokofiev, PhD Thesis, University of Zurich (2005)

[16] J. M. Butterworth *et al.*, Summary Report from the Les Houches 2009 Workshop on TeV Colliders, prep. arXiv:1003.1643 (2010)

[17] T. Rommerskirchen *et al.*, CMS Note PAS SUS-08-005

[18] T. Rommerskirchen *et al.*, CMS Note PAS SUS-09-001

[19] M. Weber *et al.*, CMS Note PAS QCD-08-003 (2008)

[20] G.L. Bayatian *et al.* (CMS Collaboration), J. Phys. G: Nucl. Part. Phys. **34** (2007) 995

[21] T. Rommerskirchen, PhD Thesis (in preparation)

2 Study of Coulomb-bound πK-pairs

C. Amsler, A. Benelli[4], C. Regenfus, and J. Rochet

In collaboration with:
CERN, Czech Technical University, Institute of Physics and Nuclear Physics Institute ASCR (Czech Republic), Laboratori Nazionali di Frascati, Messina University, Trieste University, KEK, Kyoto Sangyo University, Tokyo Metropolitan University, IFIN-HH (Bucharest), JINR (Dubna), Skobeltsin Institute for Nuclear Physics (Moscow), IHEP (Protvino), Santiago de Compostela University, Bern University.

(DIRAC Collaboration)

The goal of the DIRAC experiment at CERN (PS212) is to measure the lifetime of electromagnetically bound $\pi^+\pi^-$ or $K^\pm\pi^\mp$ pairs (the so-called $\pi\pi$- and πK- "atoms"). Their mean lives are directly related to the isospin 0 and 2 s-wave scattering lengths (a_0 and a_2) for $\pi\pi$, and to the corresponding isospin 1/2 and 3/2 scattering lengths ($a_{1/2}$ and $a_{3/2}$) for πK. More precisely, the mean life is related to the absolute value of the difference between the two scattering lengths [1], a quantity that was calculated within the framework of Chiral Perturbation Theory (ChPT) with high precision, 1.5% for $|a_0 - a_2|$ [2], and 5.5% from Roy-Steiner dispersion-relations for $|a_{1/2} - a_{3/2}|$ [3]. Thus a measurement of the mean life from DIRAC provides a valuable test of low-energy QCD concepts involving the u- and d-quarks for $\pi\pi$, and extending to the s-quark for πK. The expected mean life of πK-atoms is about 3.7 fs [1], with rather large uncertainties.

Results for $\pi\pi$-atoms have been published earlier by the DIRAC-I collaboration [4]. A mean life of $2.91^{+0.49}_{-0.62}$ fs was measured, in good agreement with predictions from ChPT. We shall focus here on πK-atoms (DIRAC-II) in which we are mainly involved.

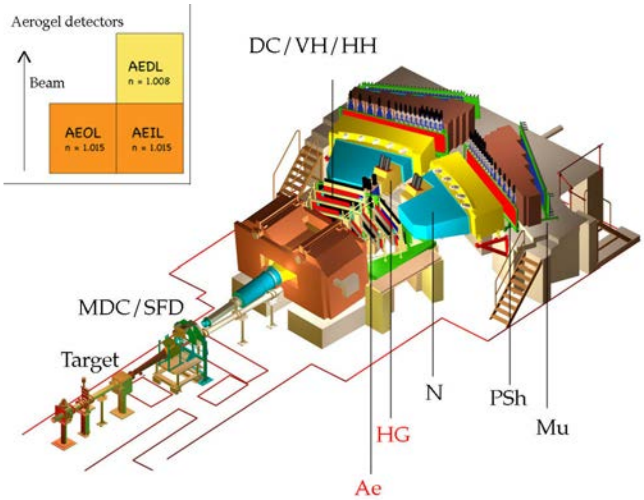

Figure 2.12: *DIRAC-II spectrometer: MDC = microdrift chambers, SFD = scintillator fibre detector, DC = drift chambers, VH, HH = vertical and horizontal scintillation hodoscopes, PSh = preshower, Mu = muon counters, Ae = aerogel, HG = heavy gas and N = nitrogen Čerenkov counters. The inset shows the arrangement of the three aerogel modules.*

A sketch of the DIRAC-II spectrometer is shown in fig. 2.12. The 24 GeV/c proton beam from the PS impinges on a thin Pt- (or Ni-) target. The secondary particles emerging from the target in the forward direction are analyzed in a double-arm magnetic spectrometer. Positive particles are deflected into the left arm, negative ones into the right arm. Electrons and positrons are vetoed by N_2-Čerenkov detectors and muons by their signals in scintillation counters behind the steel absorbers. Particle

---

[4] Visitor from JINR, Dubna

identification is performed by the heavy gas (C_4F_{10}) and aerogel Čerenkov counters. The former detects pions (but not kaons), while the latter also detects kaons (but not protons).

Our group has developed and built a large volume (37ℓ) aerogel Čerenkov counter in the left arm (positive charges) for kaon detection and proton suppression [5], and the heavy gas system [6]. The aerogel detector consists of three independent modules (inset of fig. 2.12). Two of them (AEIL close to the proton beam and AEOL at larger angles) have refractive index $n = 1.015$ and are used for kaons between 4 and 5.5 GeV/c. At small angles the momenta increase up to 8 GeV/c and hence AEDL, with the lower index $n = 1.008$, is used to suppress fast protons that also fire AEIL.

The measurement of the mean life is as follows: Atoms produced in the forward direction are ionized while crossing the target, leading to “atomic” $\pi^{\pm}K^{\mp}$-pairs with very small relative momenta between the kaons and the pions (typically < 3 MeV/c in the c.m.s system). Since ionization competes with annihilation into $K^0\pi^0$ (or $\overline{K}^0\pi^0$), the number of atomic pairs grows with increasing lifetime. Unbound πK-pairs (“Coulomb-pairs”) which interact electromagnetically are also produced. The number of produced atoms is related to the number of Coulomb-pairs [7], For relative momenta below 3 MeV/c the ratio of the number of produced atoms to that of Coulomb-pairs is around 60%. Detection efficiences are taken into account by Monte Carlo simulation. The background stems from non-Coulomb pairs due to K and π mesons from long-lived resonances (and therefore do not interact), and from accidentals (pairs produced by two different proton interactions). Figure 2.13 shows a distribution of the time difference between particles in the two arms of the spectrometer.

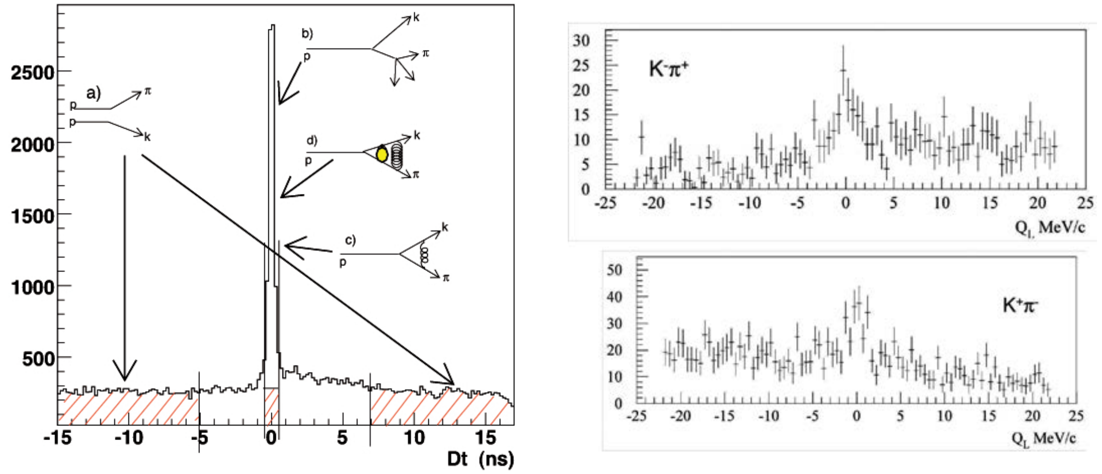

Figure 2.13: *Left: Distribution of the time difference between pions and kaons for non-Coulomb pairs (b), Coulomb-pairs (c), πK-atoms (d) and for accidentals (a). Right: Q_L distribution for selected π^+K^- and π^-K^+ events. The peak at small $|Q_L|$ is due to Coulomb- and atomic pairs (see text).*

The DIRAC collaboration observed πK-atoms for the first time with the data collected in 2007 (fig. 2.14). For comparison we also show the results for $\pi^+\pi^-$-atoms from the same data runs. We have detected 173 ± 54 πK atomic pairs [8], thus with a statistical significance of 3.2σ. However, the evidence for πK-atoms was strengthened by the simultaneous observation of Coulomb-pairs from which the fraction of expected *bound* pairs could be calculated [7]. The latter was in excellent agreement with the number of observed atoms. This result led to a lower limit for the mean life of πK-atoms of 0.8 fs in the 1s-state, at a confidence level of 90%, which could be translated into an upper limit of $|a_{1/2} - a_{3/2}| < 0.58\ m_\pi^{-1}$. Details can be found in ref. [8, 9, 10].

For the 2007 results we had used only the detectors downstream of the magnet. The kaon selection

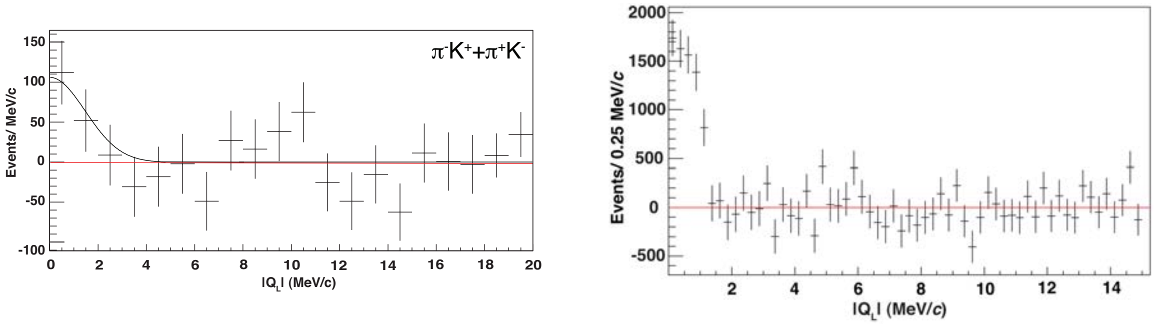

Figure 2.14: *Left: Residuals between data and the fitted background for $\pi^- K^+$ and $\pi^+ K^-$ from the 2007 data. A Gaussian fit has been applied (solid line) to illustrate the distribution of atomic-pairs. Right: Residuals between data and the fitted background for $\pi^+\pi^-$ (from ref. [9]).*

is described in detail in ref. [8, 9]. Two planes of scintillator fibers (SFD, see fig. 2.12) and 16 planes of micro drift chambers (MDC) are now available to determine the interaction point in the target with better precision. We can thus select events with relative transverse momentum smaller than 4 MeV/c, thus reducing the background by typically a factor of 4. Figure 2.13 (right) above shows the distribution of the relative longitudinal momentum Q_L for πK-pairs for a sample of the data, using the SFD planes. The enhancement at low $|Q_L|$ is due to Coulomb- (and atomic) pairs. The background for larger $|Q_L|$ is substantially lower than for data without SFD information [8].

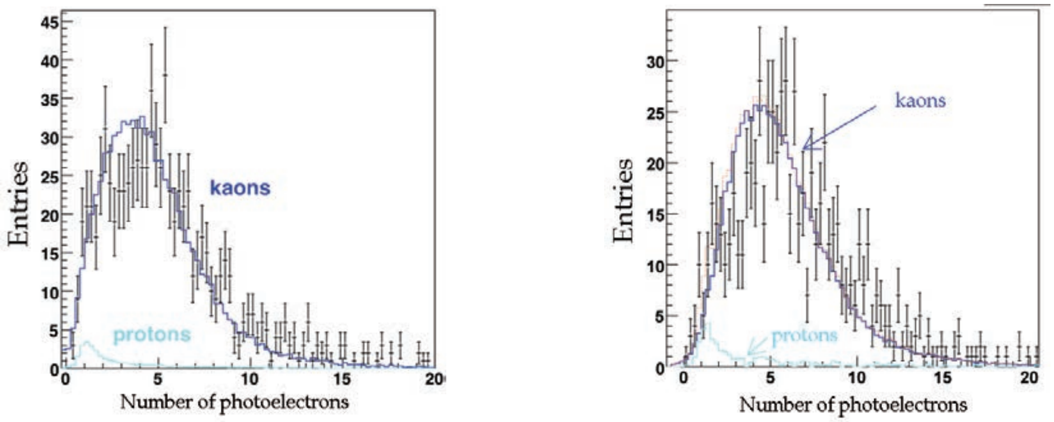

Figure 2.15: *Light yield in photoelectrons from the aerogel Čerenkov counters AEOL (left) and AEIL (right) for kaons and protons.*

In the 2007 runs ADCs for the aerogel detectors were not available. ADC and TDC information from the three aerogel modules is now recorded. To determine the light yield and detection efficiency for kaons we first selected a pure pion beam in the left arm by applying time-of-flight cuts, and also requiring a signal in the heavy gas counter. The ADC/TDC response was then analyzed as a function of pion momentum and used to estimate the response to protons. The prediction was compared to data from a pure proton beam in the left arm, applying a time-of-flight cut, requiring no signal in the heavy gas counter, and a $\pi^- p$ invariant mass consistent with the decay of a Λ-hyperon. Prediction and measurements were found to be in very good agreement. Hence the detection efficiency for kaons with the aerogel and the contamination from protons could be estimated reliably.

Figure 2.15 (left) shows the light yield for kaons and protons from the “heavy” aerogel (AEOL) in the relevant momentum range between 4.0 and 5.5 GeV/c. For example, kaons can be identified with an efficiency of 0.95 by requiring at least 2 photoelectrons, while the contamination from protons is 0.05. The results for the AEIL are similar (fig. 2.15, right). Above 5.5 GeV/c we also used the information from the "light" aerogel (AEDL) for which we obtained an average kaon efficiency of 0.95 above 5 GeV/c, while the proton contamination rose from 0.15 at 5 GeV/c to a worrying $\simeq 100\%$ above 7 GeV/c, due to the low light yield of this detector. However, a computer simulation shows that even a proton contamination at this level is not problematic: Figure 2.16 shows the $|Q_L|$ distribution for simulated $\pi^- p$ events, assuming in the reconstruction that the proton is in fact a kaon. No enhancement is observed around $Q_L = 0$, and therefore the proton contamination is automatically taken into account when subtracting the background.

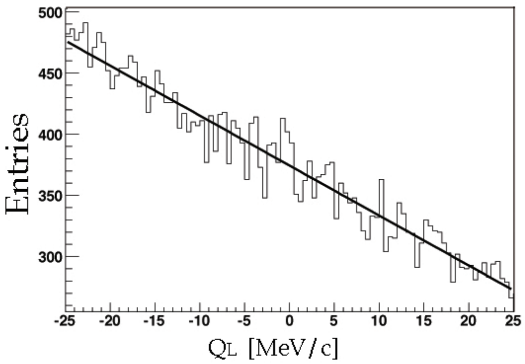

Figure 2.16: *Distribution of the longitudinal momentum difference Q_L for $p\pi^-$ events assumed to be $K^+\pi^-$.*

We collected more data in 2009. The Zurich group is currently analyzing the 2008 data sample using the new SFD detectors (provided by our Japanese collaborators), and is also implementing the corresponding Monte Carlo simulation. The SFD should improve the transverse momentum resolution from 3 MeV/c to 1 MeV/c. Data taking for DIRAC-II has been approved at least until the end of 2010 by the CERN committees, at which time we should achieve a significance of 5 – 6 standard deviations on the evidence for πK-atoms and, correspondingly, an accuracy of 40% on the lifetime (or 20% on the scattering lengths). This is a significant improvement on current knowledge, but somewhat more modest than expected, mainly due to a one year beam magnet breakdown, and the low proton beam flux that was finally delivered.

References

[1] J. Schweizer, Phys. Lett. **B587** (2004) 33
[2] G. Colangelo *et al.* Nucl. Phys. **B603** (2001) 125
[3] P. Büttiker, S. Descotes-Genon, B. Moussallam, Eur. Phys. J. **C33** (2004) 409
[4] B. Adeva *et al.* (DIRAC Collaboration), Phys. Lett. **B619** (2005) 50
[5] Y. Allkofer *et al.*, Nucl. Instr. Meth. in Phys. Res. **A582** (2007) 497;
Y. Allkofer *et al.*, Nucl. Instr. Meth. in Phys. Res. **A595** (2008) 84
[6] S. Horikawa *et al.*, Nucl. Instr. Meth. in Phys. Res. **A595** (2008) 212
[7] L. L. Nemenov, Sov. J. Nucl. Phys. **41** (1985) 629;
L. Afanasyev and O. Voskresenskaya, Phys. Lett. **B453** (1999) 302
[8] B. Adeva *et al.* (DIRAC Collaboration), Phys. Lett. **B674** (2009) 11
[9] Y. Allkofer, PhD Thesis, University of Zurich (2008)
[10] C. Amsler, Proc. of Science PoS EPS-HEP (2009) 078

3 Towards a dark matter experiment

C. Amsler, V. Boccone, W. Creus, L. Scotto Lavina, P. Otyugova, C. Regenfus, and J. Rochet

Together with the ArDM and the DARWIN Collaborations

We are constructing at CERN a 1 ton liquid argon detector (ArDM) to detect both charge and luminescence produced by recoil nuclei, following a WIMP interaction. WIMPs (Weak Interacting Massive Particles) are prime candidates for the dark matter in the universe.

Charged particles lead to ionization and excitation of argon atoms, forming excimers with the lowest singlet and the triplet excited states decaying by VUV photon emission in a narrow band around 128 nm. The singlet and the triplet states have different decay times, respectively $\tau_1 \simeq 5$ ns and $\tau_2 \simeq 1.6$ μs in liquid [1]. However, impurities such as water, air and CO_2, can absorb the VUV light and reduce τ_2 [2]. The population ratio singlet/triplet depends on ionization density. For minimum ionizing projectiles, such as electrons and γs, the ratio is ≈ 0.3, while for αs and nuclear recoils one finds a ratio of ≈ 4 [1]. Hence nuclear recoils from WIMPs populate mostly the fast decaying singlet state. In addition, the ionization yield is much lower for nuclear than for minimum ionizing particles. This is due to quick recombination which decreases the charge and enhances the luminescence. The higher ratio of light to charge production for nuclear recoils and the higher population of the fast decaying state can both be used to reduce background in WIMP searches.

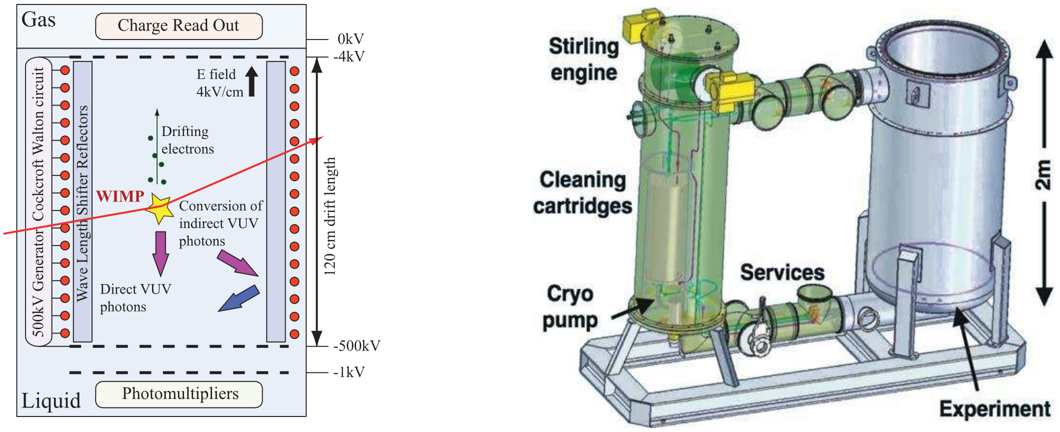

Figure 3.17: *Left: Conceptual layout of the ArDM experiment. Right: 3D sketch of the ArDM cryogenic setup with LAr cleaning circuit and main dewar.*

The ArDM experiment consists of a 1t liquid argon (LAr) detector to search for WIMPs interacting elastically with argon nuclei. A sketch illustrating the measurement principle is shown in fig.3.17. The apparatus collects signals from scintillation and ionization independently. The ionization charges drift towards the gas phase in an electric field of 4 kV/cm supplied by a Greinacher (Cockroft-Walton) chain with 210 stages. The charge is extracted from the liquid into the gas phase by a high electric field between two extraction grids (below and above the liquid surface). A large area electron multiplier (LEM) is used to amplify the charge. The field shaping rings are covered on their inner sides with reflectors to shift the 128 nm fluorescence light into the visible range and to increase the light collection efficiency [3]. Fourteen photomultipliers (PMT) are located below the HV cathode (–500 kV). The fiducial mass of the detector is estimated to be about 850 kg. The LAr recirculation and purification system (based on a CuO cartridge), provides the purity for drift distances of up to 120 cm. A 3D sketch of the detector is shown in fig. 3.17 (right).

The detector is currently installed on the surface in building 182 at CERN and our group has developed the light readout system. The ArDM detector was filled for the first time with 1 ton of LAr in May 2009 [4]. Several important parameters such as cryogenic operation at high LAr purity over weeks, stable and flawless operation of the light readout system, high scintillation light yield, and detection of events down to energies of the order of tens of keV could be verified.

The test was performed with a partial light readout assembly consisting of 7 (instead of 14) Hamamatsu R5912-MOD PMTs with Pt-underlays, no electric field and no charge readout. The PMT glass was coated with a thin layer of a transparent TPB-paraloid compound to increase the collection efficiency for VUV light. The side reflectors were made of 15 Tetratex foils $(120 \times 25\ \mathrm{cm}^2)$, coated with Tetraphenyl butadiene (TPB) wavelength shifters (WLS) of optimum thickness [5], using a custom made evaporator. The apparatus was filled with LAr with the side reflectors fully immersed and kept full for about 3 weeks, while various measurements with radioactive sources were performed.

The monitoring of the LAr purity was performed by measuring the decay time of the slow component of the light signal (τ_2) [2]. The purity was found to be constant (fig. 3.18, left), around $\tau_2 \simeq 1.5\ \mu$s, in agreement with expectations [1]. Fig. 3.18, right shows the fluctuations of the PMT calibration constants as a function of time.

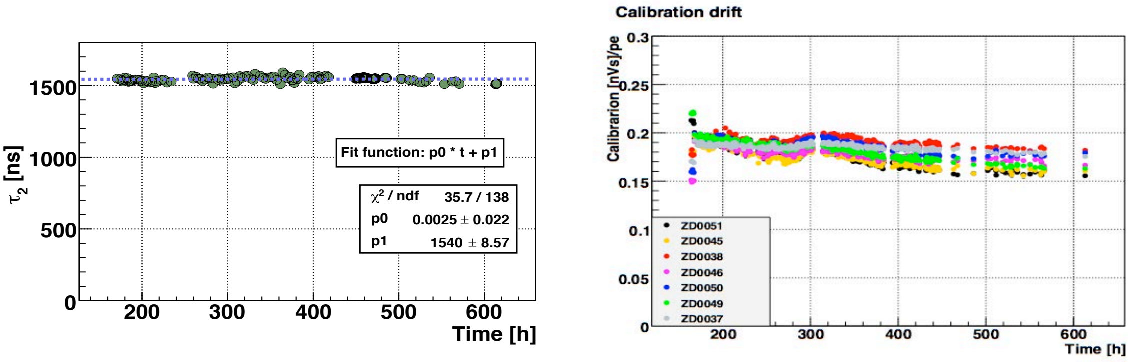

Figure 3.18: *Left: Monitoring of the LAr purity in ArDM from the slow luminescence component* τ_2 *during 600h of operation. Right: Fluctuation of the PMT calibration constants as a function of time.*

To study the detector response to γs we used a ^{22}Na source ($E_\gamma = 511$ keV and 1274 keV) and a ^{137}Cs source ($E_\gamma = 661$ keV). For ^{137}Cs the data were obtained with the LAr detector in self-trigger mode, while for ^{22}Na the detector was in coincidence with an external NaI scintillator. The response spectra are shown in fig. 3.19 (left). The shapes of the distributions can be reproduced and fitted assuming multiple Compton scattering in the detector [7]. The light yield is estimated to be ~ 0.5 photoelectrons/keV for electrons with the 7 PMTs assembly. Furthermore, by triggering on the total energy deposited by two of the three γs (511+ 1275 keV) we could select the signal from the second 511 keV γ in LAr. Fig. 3.19 (right) shows that a lower threshold of 50 keV for electrons can be reached already with 7 PMTs.

Even small neutron fluxes around 1 MeV are potentially dangerous, since the neutron-argon cross section is some 18 orders of magnitude larger than for WIMPs. It is therefore essential to investigate the response of the dark matter detector to neutrons as a function of recoil energy. We first studied the detector response to neutrons from an Am-Be source producing 3×10^4n/s neutrons in the 1 – 10 MeV range. Data were taken for different positions of the source. Figure 3.20 (left) shows the ratio CR between the integrated pulse height of the prompt light (< 50 ns) and that of the total light, as a function of integrated pulse height. These data were taken with the source located on the upper flange

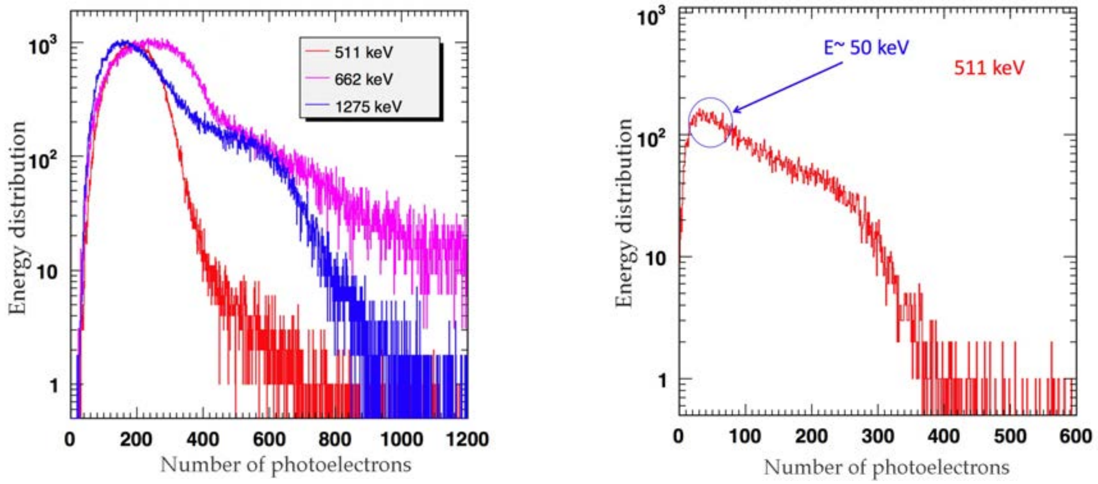

Figure 3.19: *Left: Energy spectra for* ^{137}*Cs and* ^{22}*Na. Right: Energy distribution for 511 keV* γ*s.*

of the detector. As expected, neutrons leading to the nuclear recoil band (N.R.) mainly populate the fast decaying singlet state. Figure 3.20 (left) also shows the contributions from γs leading to Compton electrons (E.R. band). The corresponding decay time distributions for the two bands are shown in fig. 3.20 (right), fitted with exponentials convoluted with Gaussians.

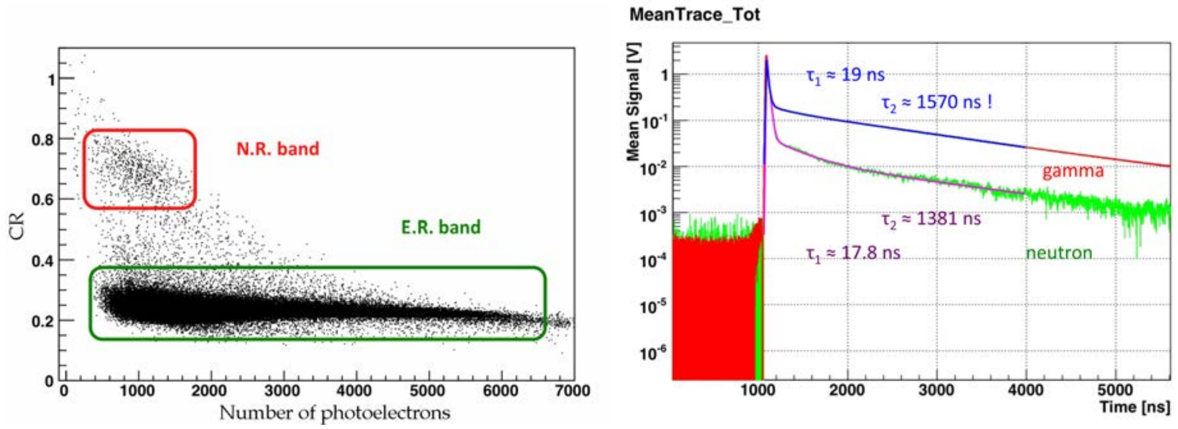

Figure 3.20: *Left: Ratio* CR *of fast to total amplitude for the Am-Be-source on the top flange of the ArDM detector. The upper box shows nuclear recoils (N.R.), the lower box electron recoils (E.R.). Right: Corresponding decay time distributions with the fast and the slow components.*

The ArDM detector was upgraded in summer 2009 to the final 14 PMTs. The deposition of WLS on the PMT windows was performed using a fast evaporation technique at the thin film laboratory of CERN. A photograph of the array under UV illumination before installation in the ArDM detector is shown in fig. 3.21. In autumn 2009 measurements were started in gaseous argon (GAr, Ar60 at room temperature and 1.1 bar pressure) using a movable ^{241}Am source (5.5 MeV αs) to obtain an estimate for the light yield with the fully equipped light readout. We collected data immediately after GAr filling to evaluate the maximum purity reached with the new turbopump system, then gathered more data as a function of time to observe the purity degradation. The best vacuum level reached before filling was 10^{-5} mbar, for which the measured slow component of the excimer-state decay τ_2 was found to be 3.04 ± 0.04 μs, in accord with known values in gas at atmospheric pressure [2]. Figure

3.21 (right) shows for each PMT with a measurement of the mean life τ_2 of the slow component, the degradation of argon purity as a function of time.

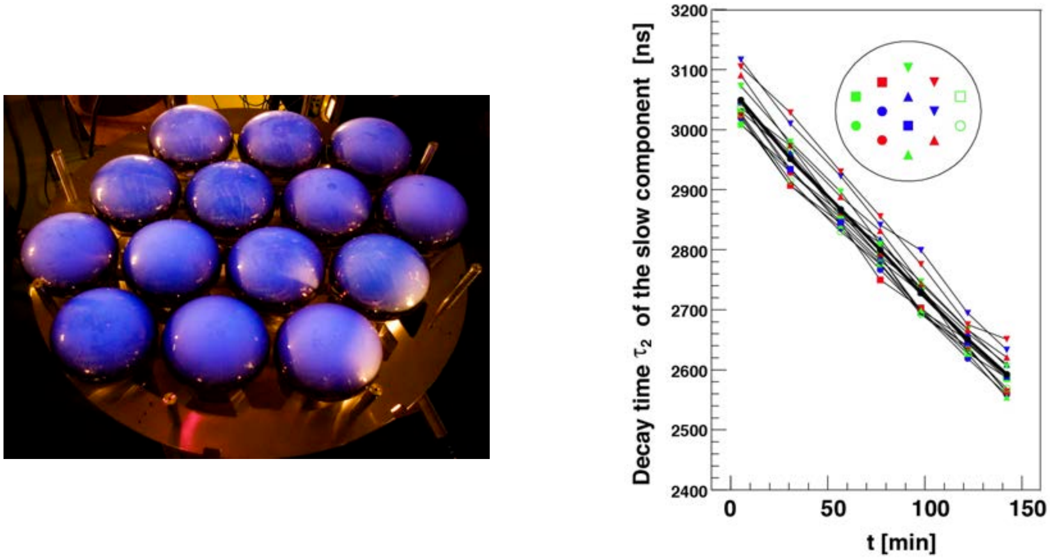

Figure 3.21: *Left: The 14 cryogenic PMTs coated with WLS, ready to be installed at the bottom of the ArDM apparatus, illuminated with UV light. Right: Measurement of the slow component of the luminescence in gaseous argon as a function of time (see text), for various source positions in the detector and for different PMTs (inset).*

We have also contributed to the online data acquisition system and to the offline software. We developed, starting from the previous existing software, and a new analysis framework to satisfy basic needs, namely easy and fast access to the data, a modular package to include the forthcoming charge readout, which can also incorporate Monte Carlo data. The package was used to analyze the late 2009 data. For example, the signal offset was previously evaluated for each event by assessing the average value of the pedestal (before event trigger time), and by rejecting events for which the width of the pedestal distribution was exceeding a preset value. In the new approach a peak finding algorithm is applied instead to the pedestal trace, searching for anomalies such as PMT dark counts, background photons, and pile-up events. Also, PMTs near the detector edges collect less light due to geometrical inefficiencies. This makes the selection of e.g. αs less inefficient from single PMTs and more prone to background. Instead, the new framework applies all cuts on the total light collected from the 14 PMTs.

As already mentioned, neutrons with energies around 1 MeV or less will contribute to the background in WIMP searches. On the other hand, radioactive neutron sources can be used to study the luminescence yield from nuclear recoils in noble liquids (fig. 3.20 above). Heavily ionizing particles such as recoiling nuclei generate significantly less light than electrons (for equal energy deposits). The quenching factor and its dependence on energy are poorly known for LAr and LXe, but lies in the range 0.15– 0.30 [8]. We intend to measure the quenching factor as a function of recoil energy down to 10 keV by studying neutron-argon and neutron-xenon scattering with monoenergetic neutrons. Furthermore, the probability for multiple neutron interactions is large (while WIMPs interact only once). This can be studied with monoenergetic neutrons in a large cell (and in ArDM). This R&D work will benefit to both ArDM and the design of a next-generation noble liquid dark matter facility in Europe (DARWIN), which was recently funded by ASPERA, and to which we participate (together with the group of Prof. L. Baudis).

Figure 3.22: *Left: Components of the neutron generator (fusion chamber, HV power supply and controller). Right: Installation in the laboratory showing the 1600 kg cylindrical shielding (grey) made of water extended polyester (WEP) mixed with a boron absorber (Colemanite,* $CaB_3O_4(OH)_3 \cdot H_2O$*).*

We have therefore purchased a neutron source from NSD-Fusion GmbH. The source delivers monoenergetic 2.45 MeV neutrons (up to 10^7 s^{-1}) from the reaction dd $\rightarrow$ He^3n. The fusion generator, designed and optimised in collaboration with the producer, was delivered at the end of 2009. The generator is based on a high voltage plasma discharge (30 - 120 kV, 1 - 15 mA). The gas pressure is controlled by heating getter disks which store the deuterium on their surfaces. Due to the excellent efficiency of the shielding the radiation dose remains far below the limit of 2.5 μSv/h at maximum fluence, and we are authorized to operate the generator at CERN without further shielding, but within a closed fence with safety and radiation interlock against X-rays, γs and neutrons (fig.3.22). The generator is routinely running in our laboratory and we are currently completing the system with a collimator, mechanical parts to hold the test chamber, and neutron detector components for the scattering experiment.

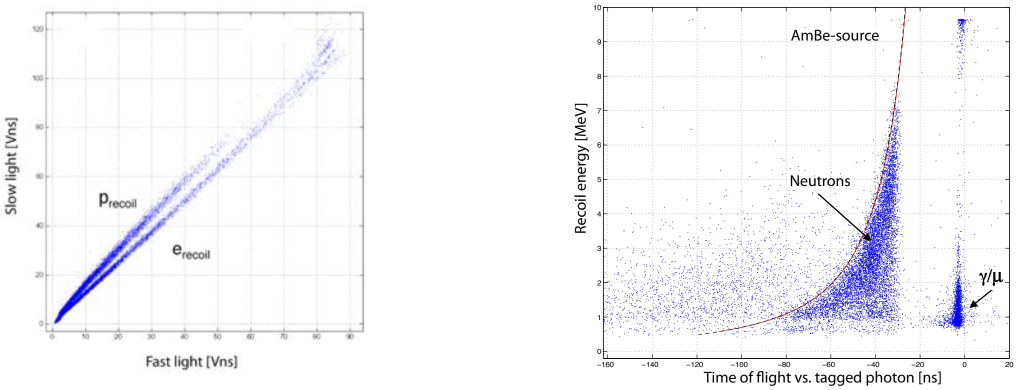

Figure 3.23: *Left: Proton and electron separation in liquid scintillator from the Am-Be source. Plotted is the distribution of integrated pulse height vs. integrated pulse height within the first 15 ns. Right: recoil proton energy vs. time-of-flight. The red line shows the expected boundary. The accumulation on the far right is due to* γ*s and cosmic muons.*

Three liquid EJ301 scintillator cells (diameters 2, 3 and 5”) were purchased from SCIONIX. They are suitable for fast neutrons ($>$ 50 keV) and give information on the neutron energy, the recoiling proton being absorbed in the cell. However, calibration is required due to the non-linearity of light output vs. proton energy. Typically half of the 2.45 MeV neutrons scatter on the carbon component and are not detected. Protons and electrons lead to different pulse shapes in the scintillator (fig. 3.23, left). A precise timing (< 1ns) can be achieved to select neutron energies by time-of-flight. We have performed measurements on the 3” detector with a 370 MBq Am-Be source located at a distance of about 1m. The source produced $3 \cdot 10^4$ n/s from the αBe reaction in the energy range 1 – 10 MeV. The neutron energy could be measured by time-of-flight by triggering on a 4.4 MeV γ (from ^{13}C* decays) emitted in coincidence, and compared with the measured proton recoil energy (fig. 3.23, right).

In the setup sketched in fig. 3.24 (left) neutrons from the dd-source are scattered in the 3” scintillation counter and detected under the angle θ by the 5” counter. Figure 3.24 (middle) shows the proton recoil spectra for neutrons in the 3” target counter which would be uniform (due to the isotropic scattering in the c.m.s.) in the absence of multiple scattering, scattering on carbon and for infinite energy resolution. Figure 3.24 (right) shows the sum of energy deposits in both counters (for θ = 45°) which should ideally be equal to the initial neutron energy. Indeed the distribution peaks around the expected incident energy of 2.5 MeV. The low energy enhancement is due to energy losses in the collimator.

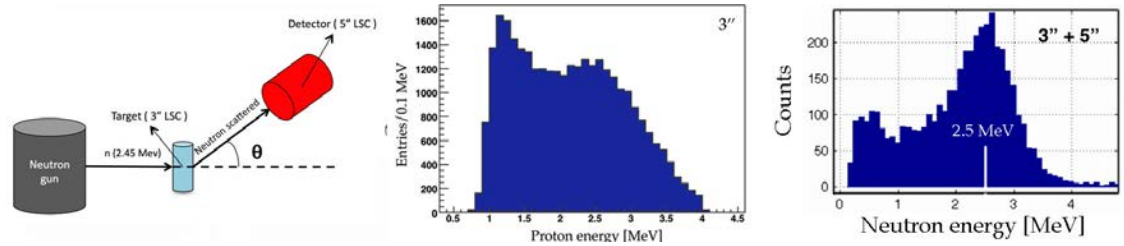

Figure 3.24: *Top: sketch of the scattering experiment. Middle: proton recoil energy distribution in the 3” target counter. Bottom: sum of the energy deposits in the 3” and 5” counters.*

R&D work for subdetector components is now being finalized and the results for the light readout efficiency are quite encouraging. The next run of the LAr detector equipped with 14 PMTs and a simple anode plane for the charge readout is planned for July 2010. This run should bring the experiment close to the point when physics operation could start. Pending are the construction and installation of the LEMs for the charge readout, and the implementation of a cryocooler and improved liquid recirculation sytem (H_2O filter). These items are in the hands of the ETHZ group. Upon completion, the detector will be moved to an underground location, probably the Canfranc underground laboratory in the Pyrenees.

References

[1] A. Hitachi *et al.*, Phys. Rev. **B27** (1983) 5279
[2] C. Amsler *et al.*, Journal of Instrumentation **3** (2008) P02001
[3] V. Boccone *et al.*, Journal of Instrumentation **4** (2009) P06001
[4] C. Amsler, Proc. 2009 Conf on HEP, Krakow (2009), PoS(EPS-HEP 2009)110;
P. Otyugova, Proc. 5th Patras Workshop on Axions, WIMPs and WISPs (2009);
C. Regenfus, Proc. TAUP 09 Conf., Rome, prep. arXiv:0912.2962v1 [phys.ins-det] (2009)
[5] H. Cabrera, Master Thesis, Universität Zürich (2007)
[6] C. Amsler *et al.*, Journal of Instrumentation **3** (2008) P02001
[7] V. Boccone, PhD thesis, Universität Zürich, in preparation
[8] D. M. Mei *et al.* Astropart. Phys. **30** (2008) 12

4 Publications

Articles

1. Mechanical design and material budget of the CMS barrel pixel detector
   C. Amsler *et al.*
   Journal of Instrumentation **4** (2009) P05003

2. Observation of πK-atoms with DIRAC-II
   Y. Allkofer
   Hyperfine Interactions **193** (2009) 39

3. Development of wavelength shifter coated reflectors for the ArDM argon dark matter detector
   V. Boccone *et al.*
   Journal of Instrumentation **4** (2009) P06001

4. Stand-alone cosmic muon reconstruction before installation of the CMS silicon strip tracker
   CMS Tracker Collaboration
   Journal of Instrumentation **4** (2009) P05004

5. ArDM, a 1t liquid argon detector for dark matter searches
   C. Amsler
   Proc. of Science PoS (EPS-HEP 2009)110

6. Experimental evidence for πK-atoms
   C. Amsler
   Proc. of Science PoS (EPS-HEP 2009) 078

7. Evidence for πK atoms with DIRAC
   A. Benelli
   Proc. of Science PoS (CD09) 008

8. Algorithms for b-Jet Identication at CMS
   A. Schmidt
   Proc. of Science PoS (EPS-HEP 2009) 439

9. The ArDM project: A Liquid Argon TPC for Dark Matter Detection
   V. Boccone
   J. Phys.: Conference Series **160** (2009) 012032

10. Test in Liquid Argon of the Light Readout System for the ArDM Experiment
    V. Boccone
    IEEE Nucl. Science Symp. Conf. Rec., Orlando N25-153 (2009)

11. Experience with CMS pixel software commissioning
    V. Chiochia
    Proceedings of Science PoS (VERTEX 2008) 010

12. Heavy Flavor Physics at CMS and ATLAS
    L. Wilke
    Proceedings of Moriond Conf. on QCD and High Energy Interactions, Ed. THE GIOI (Vietnam), 2009, p. 147

13. Searches for new phenomena at CMS and ATLAS
    T. Rommerskirchen
    Proceedings of Moriond Conf. on QCD and High Energy Interactions, Ed. THE GIOI (Vietnam), 2009, p. 171

14. Simulation and beam test measurements of the CMS pixel detector
    E. Alagöz
    Inaugural Dissertation, Universität Zürich, 2009

15. Early Observation of t-Quark in Single-Leptonic $t\bar{t}$ Decays at CMS
    D. Tsirigkas
    Inaugural Dissertation, Universität Zürich, 2009

16. Study of the B_s-Meson with the First LHC Data
    L. Wilke
    Inaugural Dissertation, Universität Zürich, 2009

17. Transverse-momentum and pseudorapidity distributions of charged hadrons in pp collisions at $\sqrt{s}$ = 0.9 and 2.36 TeV
    CMS Collaboration
    Journal of High Energy Physics **02** (2010) 041

18. Commissioning of the CMS experiment and the cosmic run at four tesla
    CMS Collaboration
    Journal of Instrumentation **5** (2010) T03001

19. Performance of the CMS Level-1 trigger during commissioning with cosmic ray muons and LHC beams
    CMS Collaboration
    Journal of Instrumentation **5** (2010) T03002

20. Performance of the CMS drift-tube chamber local trigger with cosmic rays
    CMS Collaboration
    Journal of Instrumentation **5** (2010) T03003

21. Fine synchronization of the CMS muon drift-tube local trigger using cosmic rays
    CMS Collaboration
    Journal of Instrumentation **5** (2010) T03004

22. Commissioning of the CMS High-Level Trigger with cosmic rays
    CMS Collaboration
    Journal of Instrumentation **5** (2010) T03005

23. CMS data processing workflows during an extended cosmic ray run
    CMS Collaboration
    Journal of Instrumentation **5** (2010) T03006

24. Commissioning and performance of the CMS pixel tracker with cosmic ray muons
    CMS Collaboration
    Journal of Instrumentation **5** (2010) T03007

25. Commissioning and performance of the CMS silicon strip tracker with cosmic ray muons
CMS Collaboration
Journal of Instrumentation **5** (2010) T03008

26. Alignment of the CMS silicon tracker during commissioning with cosmic rays
CMS Collaboration
Journal of Instrumentation **5** (2010) T03009

27. Performance and operation of the CMS electromagnetic calorimeter
CMS Collaboration
Journal of Instrumentation **5** (2010) T03010

28. Measurement of the muon stopping power in lead tungstate
CMS Collaboration
Journal of Instrumentation **5** (2010) P03007

29. Time reconstruction and performance of the CMS electromagnetic calorimeter
CMS Collaboration
Journal of Instrumentation **5** (2010) T03011

30. Performance of the CMS hadron calorimeter with cosmic ray muons and LHC beam data
CMS Collaboration
Journal of Instrumentation **5** (2010) T03012

31. Performance of CMS hadron calorimeter timing and synchronization using test beam, cosmic ray, and LHC beam data
CMS Collaboration
Journal of Instrumentation **5** (2010) T03013

32. Identification and filtering of uncharacteristic noise in the CMS hadron calorimeter
CMS Collaboration
Journal of Instrumentation **5** (2010) T03014

33. Performance of the CMS drift tube chambers with cosmic rays
CMS Collaboration
Journal of Instrumentation **5** (2010) T03015

34. Calibration of the CMS drift tube chambers and measurement of the drift velocity with cosmic rays
CMS Collaboration
Journal of Instrumentation **5** (2010) T03016

35. Performance study of the CMS barrel resistive plate chambers with cosmic rays
CMS Collaboration
Journal of Instrumentation **5** (2010) T03017

36. Performance of the CMS cathode strip chambers with cosmic rays
CMS Collaboration
Journal of Instrumentation **5** (2010) T03018

37. Aligning the CMS muon chambers with the muon alignment system during an extended cosmic ray run

CMS Collaboration
Journal of Instrumentation **5** (2010) T03019

38. Alignment of the CMS muon system with cosmic-ray and beam-halo muons
CMS Collaboration
Journal of Instrumentation **5** (2010) T03020

39. Precise mapping of the magnetic field in the CMS barrel yoke using cosmic rays
CMS Collaboration
Journal of Instrumentation **5** (2010) T03021

40. Performance of CMS muon reconstruction in cosmic-ray events
CMS Collaboration
Journal of Instrumentation **5** (2010) T03022

Notes/Reports

1. Algorithms for b-Jet identification in CMS
A. Schmidt *et al.*
CMS Note PAS BTV-09-001

2. Search strategy for exclusive muti-jet events from supersymmetry at CMS
T. Rommerskirchen *et al.*
CMS PAS SUS-09-001

3. Algorithms for Identification of jets containing b-quarks
C. Saout and A. Schmidt
CMS Times, 7 September 2009

4. Kaon/proton separation with the aerogel
A. Benelli and V. Yazkov
DIRAC note 09-07

Articles in press

1. The tools and Monte Carlo Working group (summary report).
J. Alwall *et al.*
Proc. of the les Houches 2009 Workshop on Tools and Monte Carlo
Prep. arXiv:1003.1643v1 [hep-ph]

2. Development and test in liquid argon of the light readout system for the ArDM experiment
V. Boccone
Proc. of the Tenth Conf. on the Intersections of Part. and Nucl. Phys. (CIPANP 2009), San Diego

3. Study of the B_s meson with forthcoming LHC data at CMS
B. Millán Mejías
Proc. of the VIII Latin Am. Symp. on Nucl. Phys. and Appl., Santiago de Chile

4. The ArDM, a ton-scale liquid argon experiment for direct Dark Matter detection
P. Otyugova
Proc. of the 5th Patras Workshop on Axions, WIMPs and WISPs, Durham (2009)

5. The ArDM - a ton-scale liquid argon experiment for direct Dark Matter detection
   P. Otyugova
   Proc. of the Invisible Universe Int. Conf., Paris (2009)

6. The Argon Dark Matter Experiment (ArDM)
   C. Regenfus
   Proc. of the Conf. on Topics in Astroparticle and Underground Physics (TAUP 09), Rome
   Prep. arXiv:0912.2962v1 [physics.ins-det]

Lectures

1. C. Amsler
   Seminar, Tata Institute of Fundamental Research (TIFR), Mumbai
   9 November 2009
   “ArDM, a large liquid argon detector for dark matter searches”

2. C. Amsler
   Colloquium, Tata Institute of Fundamental Research (TIFR), Mumbai
   11 November 2009
   “From antihydrogen production to dark matter searches, some experimental aspects”

3. A. Benelli
   6th Int. Workshop on Chiral Dynamics, Bern
   6 July 2010
   “Evidence for $K\pi$ atoms with DIRAC”

4. V. Boccone
   Tenth Conference on the Intersections of Part. and Nucl. Phys. (CIPANP 2009), San Diego
   27 May 2009
   “Development and test in liquid argon of the light readout system for the ArDM experiment”

5. V. Chiochia
   SPS/ ÖPG meeting, Innsbruck,
   3 September 2009
   “Study of the CMS experiment at the Large Hadron Collider”

6. C. Favaro
   Contributed talk, CHIPP PhD Winter School 2010, Monte Verità, Ascona
   24 January 2010
   “The phase 1 upgrade of the CMS silicon pixel detector”

7. M. Ivova Rikova
   Contributed talk, CHIPP PhD Winter School 2010, Monte Verità, Ascona
   24 January 2010
   “Measurements of the Lorentz angle in the CMS barrel pixel detector with collision and cosmic data”

8. A. Jaeger
   Contributed talk, CHIPP PhD Winter School 2010, Monte Verità, Ascona
   24 January 2010
   “Commissioning of the CMS pixel detector using first data”

9. B. Millán Mejías
   Invited talk, Proc. of the VIII Latin Am. Symp. on Nucl. Phys. and Appl., Santiago de Chile
   18 December 2009
   "Study of the Bs meson with first LHC data at CMS".
10. P. Otyugova
    Invisible Universe International Conference 2009, Paris
    1 July 2009
    "The ArDM (CERN RE 18) – a ton-scale liquid argon experiment for direct Dark Matter detection"
11. P. Otyugova
    5th Patras Workshop on Axions, WIMPs and WISPs
    16 July 2009
    "The ArDM, a ton-scale liquid argon experiment for direct Dark Matter detection"
12. C. Regenfus
    Conf. on Topics in Astroparticle and Underground Physics (TAUP 09), Rome
    1 July 2009
    "The Argon Dark Matter Experiment (ArDM)"
13. C. Regenfus
    SPS/ ÖPG meeting, Innsbruck,
    2 September 2009
    "The AEgIS experiment at CERN: Dropping antihydrogen atoms"
14. C. Regenfus
    Presentation at the Scientific Commitee meeting, Laboratorio Subterráneo de Canfranc
    22 October 2009
    "1 ton liquid argon TPC/calorimeter for direct detection of DM"
15. S. de Visscher
    CMS Plenary talk
    16 March 2010
    "Overview of the pixel performance results from 900 GeV run and program for 7 TeV"
16. S. de Visscher
    Spring plenary meeting of the GDR Terascale meeting, Saclay
    30 March 2010
    "Unconventional phenomenology of a minimal two-Higgs-doublet model"

ArDM Collaboration (2009):
C. Amsler, A. Badertscher, V. Boccone, A. Bueno, H. Cabrera, M. C. Carmona-Benitez, M. Daniel , E. J. Daw, U. Degunda, A. Dell'Antone, A. Gendotti, L. Epprecht, S. Horikawa, L. Kaufmann, L. Knecht, M. Laffranchi, C. Lazzaro, P. K. Lightfoot, D. Lussi, J. Lozano, A. Marchionni, K. Mavrokoridis, A. Melgarejo, P. Mijakowski, G. Natterer, S. Navas-Concha, P. Otyugova, M. de Prado, P. Przewlocki, C. Regenfus, F. Resnati, M. Robinson, J. Rochet, L. Romero, E. Rondio, A. Rubbia, N. J. C. Spooner, T. Strauss, J. Ulbricht, T. Viant.

DIRAC Collaboration (2009):
B. Adeva, L. Afanasyev, Y. Allkofer, C. Amsler, A. Anania, A. Benelli, V. Brekhovskikh, G. Caragheorgheopol, T. Cechak, M. Chiba, P. Chliapnikov, C. Ciocarlan, S. Constantinescu, C. Curceanu,

C. Detraz, D. Dreossi, D. Drijard, A. Dudarev, M. Duma, D. Dumitriu, J.L. Fungueiriño, J. Gerndt, A. Gorin, O. Gorchakov, K. Gritsay, C. Guaraldo, M. Gugiu, M. Hansroul, Z. Hons, S. Horikawa, M. Iliescu, V. Karpukhin, J. Kluson, M. Kobayashi, V. Komarov, V. Kruglov, L. Kruglova, A. Kulikov, A. Kuptsov, I. Kurochkin, K.-I. Kuroda, A. Lamberto, A. Lanaro, V. Lapshin, R. Lednicky, P. Levi Sandri, A. Lopez Aguera, V. Lucherini, I. Manuilov, C. Mariñas, L. Nemenov, M. Nikitin, K. Okada, V. Olchevskii, M. Pentia, A. Penzo, M. Pló, G.F. Rappazzo, C. Regenfus, J. Rochet, A. Romero, V. Ronjin, A. Ryazantsev, V. Rykalin, J. Saborido, J. Schacher, A. Sidorov, J. Smolik, S. Sugimoto, F. Takeutchi, A. Tarasov, L. Tauscher, T. Trojek, S. Trusov, V. Utkin, O. Vázquez Doce, T. Vrba, V. Yazkov, Y. Yoshimura, M. Zhabitsky, P. Zrelov.

PARTICLE DATA Group (2008):
C. Amsler, M. Doser, M. Antonelli, D. Asner, K.S. Babu, H. Baer, H.R. Band, R.M. Barnett, J. Beringer, E. Bergren, G. Bernardi, W. Bertl, H. Bichsel, O. Biebel, P. Bloch, E. Blucher, S. Blusk, R.N. Cahn, M. Carena, C. Caso, A. Ceccucci, D. Chakraborty, M.-C. Chen, R.S. Chivukula, G. Cowan, O. Dahl, G. D'Ambrosio, T. Damour, A. de Gouvea, T. DeGrand, B. Dobrescu, M. Drees, A. Edwards, S. Eidelman, V.D. Elvira, J. Erler, V.V. Ezhela, J.L. Feng, W. Fetscher, B.D. Fields, B. Foster, T.K. Gaisser, L. Garren, H.-J. Gerber, G. Gerbier, T. Gherghetta, G.F. Giudice, M. Goodman, C. Grab, A.V. Gritsan, J.-F. Grivaz, D.E. Groom, M. Grnewald, A. Gurtu, T. Gutsche, H.E. Haber, K. Hagiwara, C. Hagmann, K.G. Hayes, J.J. Hernández-Rey, K. Hikasa, I. Hinchliffe, A. Höcker, J. Huston, P. Igo-Kemenes, J.D. Jackson, K.F. Johnson, T. Junk, D. Karlen, B. Kayser, D. Kirkby, S.R. Klein, I.G. Knowles, C. Kolda, R.V. Kowalewski, P. Kreitz, B. Krusche, Yu.V. Kuyanov, Y. Kwon, O. Lahav, P. Langacker, A. Liddle, Z. Ligeti, C.-J. Lin, T.M. Liss, L. Littenberg, J.C. Liu, K.S. Lugovsky, S.B. Lugovsky, H. Mahlke, M.L. Mangano, T. Mannel, A.V. Manohar, W.J. Marciano, A.D. Martin, A. Masoni, D. Milstead, R. Miquel, K. Mönig, H. Murayama, K. Nakamura, M. Narain, P. Nason, S. Navas, P. Nevski, Y. Nir, K.A. Olive, L. Pape, C. Patrignani, J.A. Peacock, A. Piepke, G. Punzi, A. Quadt, S. Raby, G. Raffelt, B. Renk, P. Richardson, S. Roesler, S. Rolli, A. Romaniouk, L.J. Rosenberg, J.L. Rosner, C.T. Sachrajda, Y. Sakai, S. Sarkar, F. Sauli, O. Schneider, D. Scott, B. Seligman, M. Shaevitz, T. Sjöstrand, J.G. Smith, G.F. Smoot, S. Spanier, H. Spieler, A. Stahl, T. Stanev, S.L. Stone, T. Sumiyoshi, M. Tanabashi, J. Terning, M. Titov, N.P. Tkachenko, N.A. Törnqvist, D. Tovey, G.H. Trilling, T.G. Trippe, G. Valencia, K. van Bibber, M.G. Vincter, P. Vogel, D.R. Ward, T. Watari, B.R. Webber, G. Weiglein, J.D. Wells, M. Whalley, A. Wheeler, C.G. Wohl, L. Wolfenstein, J. Womersley, C.L. Woody, R.L. Workman, A. Yamamoto, W. -M. Yao, O.V. Zenin, J. Zhang, R.-Y. Zhu, P.A. Zyla.

CMS Collaboration:
see http://cms.web.cern.ch/cms/Collaboration/Institutes/index.html